GEOPHYSICAL RESEARCH LETTERS, VOL. 24, NO. 21, PAGES 2635-2638, NOVEMBER 1, 1997

Infrared glow above thunderstorms?

R. H. Picard,[1] U. S. Inan,[2] V. P. Pasko,[2] J. R. Winick,[1] and P. P. Wintersteiner[3]

Abstract. Sustained heating of lower ionospheric electrons by thundercloud fields, as recently suggested by *Inan et al.* [1996], may lead to the production of enhanced infrared (IR) emissions, in particular 4.3-μm CO_2 emission. The excitation rate for N_2(v) via electron collisions is calculated using a new steady-state two-dimensional electrostatic-heating (ESH) model of the upward coupling of the thundercloud (TC) electric fields. The vibrational energy transfer to CO_2 and 4.3-μm radiative transfer are then computed using a line-by-line non-LTE (non-local thermodynamic equilibrium) radiation model. Limb-viewing radiance profiles at 4.3-μm and typical radiance spectra are estimated for five different TC charge distributions and ambient ionic conductivities. Broadband 4.3-μm enhancements of greater than a factor of two above ambient nighttime levels are predicted for tangent heights (TH) in the range ~80 to >130 km for the most perturbed case, with larger enhancements in selected narrower spectral regions. The predicted IR enhancements should be observable to an orbiting IR sensor.

Introduction

Thunderstorms are thought to be the batteries for the global electric circuit [*Hays and Roble*, 1979; *Roble*, 1991]. Intense quasi-electrostatic (QE) TC fields which exist during brief (~10 ms) periods following lightning discharges are now believed to heat the free electrons at 50-90 km altitude, leading to the production of new molecular excitation and optical emissions (sprites) [*Pasko et al.*, 1997]. In addition to the visible and near-IR emission from short-lived states, notably N_2 first-positive emission [*Mende et al.*, 1995; *Hampton et al.*, 1996], which are efficiently produced by the transient QE heating, the possibility also exists to generate IR rovibrational emissions, such as the 4.3-μm ν_3 bands of CO_2 or the 5.3-μm fundamental and the 2.7-μm overtone bands of NO [*Whalen et al.*, 1985]. However, the long lifetimes of the IR radiating states (~ 0.1 s) compared to the duration of the transient QE fields makes QE heating relatively ineffective in producing IR emissions.

On the other hand, it has recently been realized that, even under the quasi-steady conditions between lightning discharges, TC fields can maintain the ionospheric electrons in a heated state [*Inan et al.*, 1996]. Although the quiescent fields penetrating to ionospheric altitudes are relatively smaller than the transient fields which produce sprites, they are nevertheless believed to heat electrons significantly [*Pasko et al.*, 1996]. In this paper, we consider one of the possible consequences of such steady and sustained heating, namely the steady-state excitation of IR emissions.

To determine the amount of sustained heating at 70-90 km altitude, it is necessary to model self-consistently the penetration of TC electric fields E to the upper atmosphere. Previous considerations of this problem [*Park and Dejnakarintra*, 1973; *Tzur and Roble*, 1985; *Roble*, 1991; *Velinov and Tonev*, 1995] have not accounted for the nonlinear dependence on $|E|$ of the ionospheric-electron conductivity $\hat{\sigma}_e$ due to electron heating. Here we use the recently developed two-dimensional self-consistent electrostatic heating (ESH) model of *Pasko et al.* [1996] to determine the E-field penetration and the resultant electron heating. An important consequence of the heating is the excitation of non-radiating N_2 vibrational levels, which we determine quantitatively as a function of altitude. The N_2 vibrational energy transfers efficiently to CO_2 ν_3 vibrational states, which then radiate at 4.3 μm. We use the calculated N_2 vibrational excitation rates in the ARC non-LTE radiative-transfer code [*Wintersteiner et al.*, 1992; *Nebel et al.*, 1994] to determine CO_2 ν_3 excitation and the resultant IR emission levels.

N_2 Vibrational Excitation

The ESH model of *Pasko et al.* [1996] assumes cylindrical symmetry about the z-axis (altitude) and describes the steady-state (that is, static) electric field established in the atmosphere due to a vertical TC dipole charge configuration, consisting of two charges of $+Q$ and $-Q$ separated in altitude above a perfectly conducting ground at $z = 0$. The E field is calculated using the stationary charge continuity equation, in which TC charges play the role of steady current sources, assumed to be maintained against conduction loss by external means, for example updrafts or other meteorological processes. The nonlinear heating effects on $\hat{\sigma}_e$ of the medium above the TC are calculated self-consistently by solving the nonlinear continuity equation.

Each of the dipole charges $\pm Q$ is taken to be distributed in the form of spherical or disk-shaped clouds centered at altitude $z_o^{\pm}$ and of width $2a$. The spherical distributions have positive and negative charge densities $\propto e^{-[(z-z_o^{\pm})^2+r^2]/a^2}$, where r is the radial cylindrical coordinate, a=3 km, z_o^-=5 km, and z_o^+=15 km. For disk-shaped TC charge distributions, such as those which exist in a mesoscale convective system (MCS) [for example, *Marshall et al.*, 1996], the charge density is $\propto e^{-[(z-z_o^{\pm})^2]/a^2}$ (a=3 km) and is uniform in the r direction out to the radius of the disk. Larger E fields will result everywhere above the cloud if either z_o^+ or $|z_o^+ - z_o^-|$ is increased.

An important parameter that determines the penetration of the TC fields to high altitudes is the scale height of the upper-atmospheric conductivity σ. At altitudes below ~60 km, the atmospheric conductivity is largely determined by the ion component σ_i, which is not significantly modified by ESH. Nevertheless, altitude profiles of σ_i are not well known, especially above an active thunderstorm, and available *in situ* data from rockets [for example, *Hale et al.*, 1981] indicate large variability. Accordingly, we provide results for different ambient σ_i profiles. At altitudes above ~60 km, the electron component $\hat{\sigma}_e$ is dominant. Although the ambient profiles of electron density are also not well known, results are less sensitive to the assumed ambient profiles in this altitude range, since the electron conductivity is reduced self-consistently by ESH. The electrostatic fields penetrating to high altitudes are generally of low intensity, so that neither ionization effects nor excitation of optical emissions need be considered. Note that the type of coupling considered here occurs during the entire duration of the thunderstorm, including the times between lightning discharges.

With the electrostatic field self-consistently determined as a function of altitude, the electron distribution function is readily estimated using a kinetic formulation [*Taranenko et al.*, 1993] by accounting for all electron collisional losses,

[1]Phillips Laboratory / Geophysics, Hanscom AFB, Mass.
[2]STAR Laboratory, Stanford University, Stanford, Calif.
[3]ARCON Corporation, Waltham, Mass.

Copyright 1997 by the American Geophysical Union.

Paper number 97GL02753.
0094-8534/97/97GL-02753$05.00

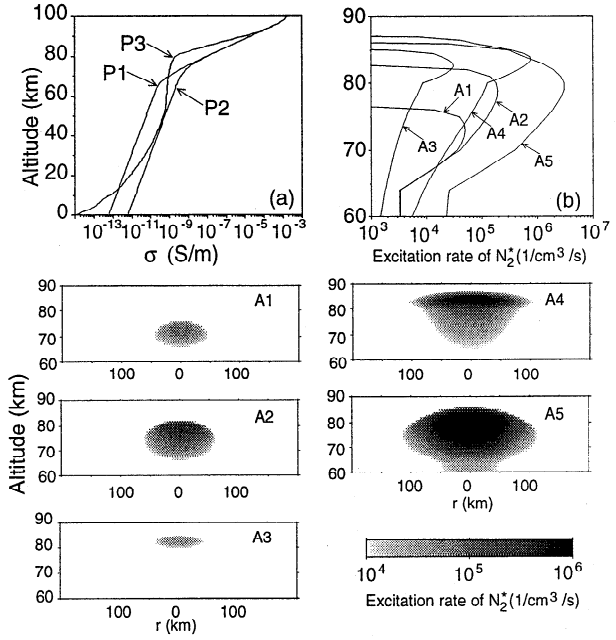

Figure 1. (a) Three models of ambient electrical conductivity σ. (b) Altitude profiles and (c) spatial distributions of $N_2(v)$ excitation rate due to heated electrons.

including the very important loss due to vibrational excitation of N_2. The excitation rates for $N_2(v)$ can then be determined using well-known cross sections [*Phelps*, 1987]. For numerical calculations, we use parametrized production rates of vibrationally excited N_2 as a function of E/N (where E is the electric field and N is the neutral number density) [*Pasko et al.*, 1997].

We consider three different nighttime ambient conductivity profiles P1, P2, and P3 (Figure 1a). Profile P1 consists of an ion conductivity profile with a constant scale height of 11 km and an electron conductivity calculated from a typical D-region electron-density profile used in previous work [*Inan et al.*, 1996]. Profile P2 has the same scale height as P1, but has an ionic conductivity ten times larger at each altitude. Profile P3 is probably the most 'typical' midlatitude profile and is based on a range of rocket measurements [*Hale*, 1994, and references therein]. Profiles P1 and P2 bracket the range of variations of σ at altitudes ~60 km.

We combine the three different conductivity profiles with the two different TC charge configurations into five cases which span the range of interest. The five cases are: (i) A1 - spherical, $Q = \pm 100$ C, σ profile P1; (ii) A2 - same as A1, but with σ profile P2; (iii) A3 - same as A1, but with σ profile P3; (iv) A4 - disk-shaped, radius = 50 km, $Q = \pm 1000$ C, σ profile P3; and (v) A5 - same as A4, but with σ profile P2. TC charges of 100 C are not uncommon [for example, *Brook et al.*, 1982]. Moreover, the effective surface charge density corresponding to 1000 C spread over a disk with radius 50 km is ~130 nC/m^2, several times lower than the values of 400-1200 nC/m^2 suggested by *Marshall et al.*[1996] for a MCS. Thus, the TC charge magnitudes used in our calculations are quite conservative.

Figure 1b shows altitude profiles (at r=0) of the vibrational excitation rate of $N_2(v)$ corresponding to the different cases. The lateral extent of the regions which are excited are indicated for each case separately in the panels of Figure 1c. Comparison of results for Cases A2 and A1 illustrate that higher conductivity values at lower altitudes (Case A2) allow for better upward penetration of fields and higher field values. However, the most effective coupling is obtained for disk-like TC charge distributions as represented by A4 and A5. The largest perturbations are produced for Case A5, which also provides for the penetration of the electrostatic field to the highest altitude. In Cases A4 and A5 electric fields $E \sim$ 1-10 V/m are produced near z = 80 km. Such fields are too low to produce significant ionization. In all cases electron densities are near ambient values.

CO_2 ν_3 Vibrational Temperatures

We determine the populations of the ν_3 excited states using a line-by-line non-LTE model [*Wintersteiner et al.*, 1992], in which rate equations for the level populations and the equation of transfer for the radiative flux are solved simultaneously. The extended duration of the TC fields makes it possible to use a steady-state formulation, which ignores transient radiative behavior. We consider the combined effects of electron collisional excitation and the ambient nighttime production/loss processes of *Nebel et al.* [1994].

In steady state, the main pathway for CO_2 ν_3-state excitation by heated electrons is indirect, involving vibration-to-vibration (V-V) transfer from electron-excited $N_2(v)$, calculated in the previous section. This follows from (i) the abundance of N_2, (ii) the long lifetime of the $N_2(v>0)$ states, and (iii) the efficient near-resonant V-V transfer process. The near-resonance requires that the rate equations be solved simultaneously for the $CO_2(\nu_3)$ and $N_2(v)$ excited-vibrational-state populations. The stored N_2 vibrational excitation is initially transferred, with a time constant of a few seconds at 70 km to a minute at 90 km, to CO_2 ν_3 vibrational states, which then radiate rapidly at 4.3 μm (lifetime ~2.5 ms). However, in the mesosphere the effective CO_2 excited-state lifetime and the $N_2(v)$ relaxation time are both lengthened considerably by radiation trapping and by the reverse V-V process, whereby the vibrational excitation is passed back to N_2. Effective $N_2(v)$ relaxation times are in the range 5-7 min at 70-90 km altitude [*Kumer*, 1977].

While the vibrational energy is redistributed locally by V-V transfer, it is also being redistributed nonlocally by radiative transport. We allow vertical radiative transfer, but neglect horizontal radiative transport/diffusion of the excitation, since the horizontal scale (lateral extent of the TC charge) is much larger than the vertical scales (neutral-density and enhanced-E-field scale height). At 80 km altitude, radiation will only diffuse horizontally a few km in 20 min, negligible compared to the width of the charge distribution. Moreover, one must include in the computation a number of weaker isotopic and hot bands, since they account for most of the radiative redistribution of the excitation over altitude and most of the limb radiance at 80 km TH, the stronger bands being severely self-absorbed.

In our model calculations, we consider four CO_2 isotopes and five excited states. We include the most abundant 626 isotope, along with the minor isotopes 636, 627, and 628, and the excited states 00011, 01111 (which radiates the first hot band), and the states we shall call Group I (10011, 10012, and 02211). The notation for the CO_2 states and isotopes is given by *Nebel et al.* [1994] and by *Rothman et al.* [1992]. We assume (1) nighttime conditions, (2) a midlatitude model atmosphere similar to the U.S. Standard Atmosphere (1976), (3) non-overlapping spectral lines, and (4) local rotational equilibrium within a band at the kinetic temperature T. We express non-LTE vibrational populations in terms of a vibrational temperature $T_{\rm vib}$ [*Nebel et al.*, 1994].

The altitude profiles of $T_{\rm vib}$ were calculated for all bands of interest, and representative profiles are shown in Figures 2a-c for the unheated atmosphere and Cases A4 and A5, respectively. Results for Cases A1-A3 are not shown since enhancements were small. In each case, the T profile is shown, as well as $T_{\rm vib}$ profiles for N_2(v=1) and five CO_2 states. In the ambient case we see that $T_{\rm vib} > T$ for the strongly non-LTE CO_2 states in the mesopause region, since the production is dominated by radiative excitation. The less abundant isotopes are vibrationally hotter because they are optically thinner and are excited by radiation originating further away near the warm stratopause. In the lower thermosphere, on the other hand, $T_{\rm vib} < T$ for the CO_2 states because radiative loss (cooling to space) dominates. The $T_{\rm vib}$ profile for N_2 is locked to the CO_2 00011 626 $T_{\rm vib}$ in the mesosphere due to the strong V-V transfer. On the other hand, in the thermosphere it is locked to T, because the time constant for V-V transfer becomes very long and the $N_2(v)$ loss is then dominated by collisions with O.

When the electrons are heated, enhancements of $T_{\rm vib}$ occur above 70 km and are strongest at 80 km near the peak of $N_2(v)$ excitation by electrons. The enhancements are quite modest (~10 K) for Case A2 (not shown), but approach 50

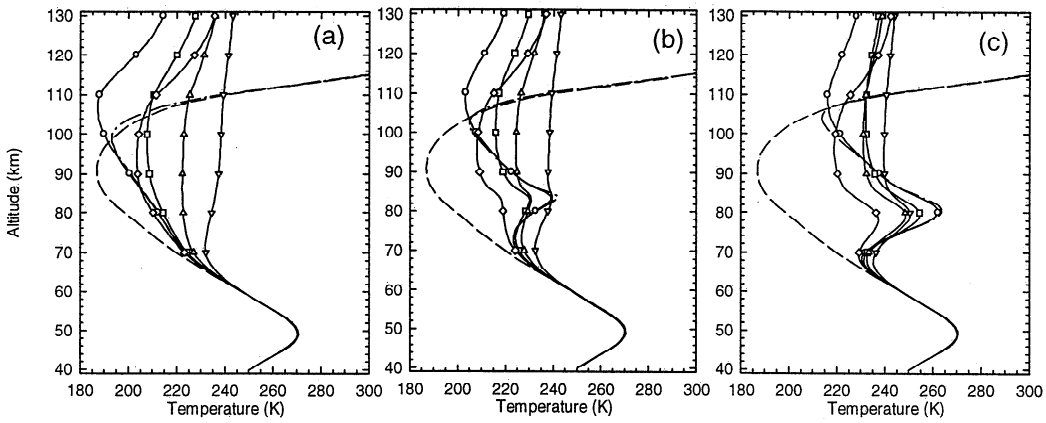

Figure 2. Altitude profiles of $T_{\rm vib}$ (a) for unheated conditions, (b) for Case A4, and (c) for Case A5. Symbols designate CO_2 isotopes and states as follows: ○ (626 00011), □(636 00011), △ (628 00011), ▽ (627 00011), ◇ (626 01111). Profiles of T (dashed) and N_2(v=1) $T_{\rm vib}$ (dash/double-dot) are also shown.

K for Case A5. An increase of 10 K (50 K) corresponds to a factor of ~2 (~17) increase in the upper-state population at $T_{\rm vib}$ = 220 K. A significant feature of the enhancements is that they occur not only in the region of enhanced N_2(v) excitation below 85 km, but extend up into the thermosphere, well above 130 km. The responsible mechanism is IR radiative diffusion of the excitation upward from the region of enhanced production. A similar process is effective in redistributing auroral electron energy deposited in N_2 vibration [*Winick et al.*, 1988]. The 626 and 636 01111 states also show significantly enhanced $T_{\rm vib}$, but the Group I excited-state enhancements (not shown) are negligible.

CO_2 4.3-μm Limb Radiance

We now calculate the enhanced 4.3-μm radiance in limb view for LOS with tangent points located at r=0. The calculation includes segments on both the near and far side of the tangent point where ambient conditions prevail.

Figure 3a shows the nighttime limb radiance profiles for Cases A4 and A5 and for ambient conditions, for a sensor with an infinitesimal field-of-view and a wide spectral passband (4.1-4.5 μm). Cases A1-A3 (not shown) are nearly indistinguishable from the ambient, but enhancements of up to ~20% and ~100% occur for cases A4 and A5, respectively. Near-peak enhancements occur over a broad range of TH from ~76 km to >120 km, extending well above the region of E-field-enhanced production. Figure 3b shows the enhancement ratio for individual bands as a function of TH for Case A5, demonstrating that the enhancement profile depends strongly on the band. The altitude dependence is much stronger for the 626 00011-00001 (main) band, since its optical thickness prevents radiative diffusion of the enhanced production. On the other hand, the two strongest minor bands, 636 00011-00001 and 626 01111-01101, have broader enhancement profiles, due to the increased radiative diffusion. Near the altitude of peak vibrational excitation (~80 km), the main-band enhancement dominates, while in the lower thermosphere the two weaker bands have enhancements nearly equal to each other and to the main band. Although the main-band radiance is larger by as much as a factor of six at ~80 km, it only accounts for 5-10% of the radiance there, since it is severely self-absorbed. This is illustrated in Figure 3c, which shows the fraction of the total limb radiance under ambient conditions originating from the main 626 band, all of the isotopic 00011-00001 bands, the first 626 hot band, and other hot bands (largely first hot bands of minor isotopes and bands arising from Group I states). The main 626 band makes the largest contribution only below 62 km and above 105 km, while the minor-isotope 00011-00001 bands dominate the radiance from 73 to 105 km.

The variation in optical thickness of the bands and the dependence of the enhancement ratios on TH lead to interesting spectral behavior, which may be detectable with a limb-looking narrowband multichannel radiometer or with an IR spectrometer. In Figure 4 we show typical spectra for the ambient atmosphere and for Case A5 at 80 km TH. The spectrum is plotted for an instrumental resolution of 2 cm^{-1} and shows considerable structure, including band origins, sharp Q-branches, and broader P- and R-branches. It is clear that spectral-radiance enhancements are dependent on wavenumber and that diverse spectral features are enhanced differently. While the integrated radiance more than doubles, the increase within limited spectral regions, such as the 'blue spike' region near 2380 cm^{-1}, can be con-

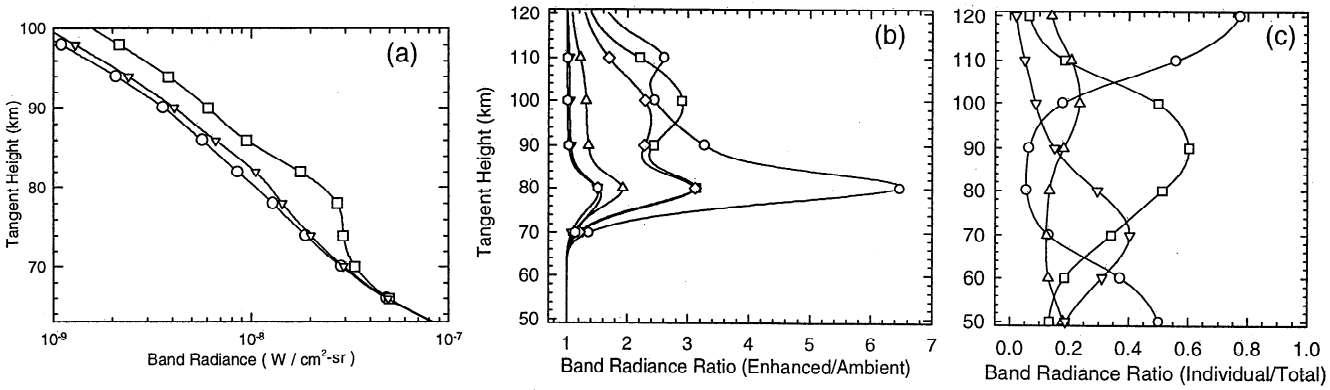

Figure 3. (a) Total limb radiance profiles for ambient nighttime and Cases A4 and A5. (b) Heating enhancement ratios for limb radiance in a number of bands versus TH for Case A5. Symbols for upper states of bands same as in Figure 2, except that curve is added (hexagons) for hot bands originating in states other than 626 01111. (c) Profiles of fractional limb radiance in certain band groups for ambient nighttime. Upper (radiating) level designations are: ○ (00011 626), □(00011 minor isotopes), △ (626 01111 hot band), ▽ (states radiating other hot bands).

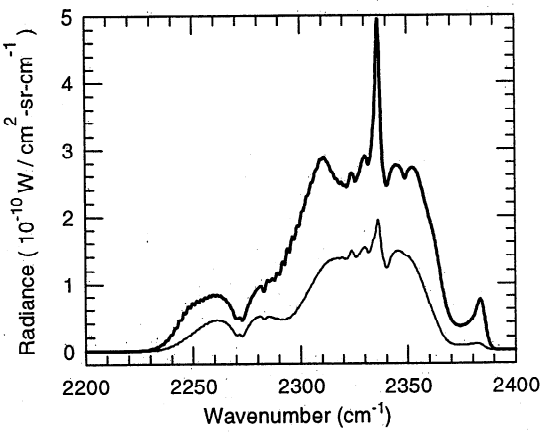

Figure 4. 4.3-μm limb spectra for TH = 80 km: Ambient night (thin), Case A5 (thick).

siderably larger. Larger effects are also possible when the heated region is on the side of the tangent point nearer the sensor.

Summary and Discussion

Our results indicate that sustained heating of lower ionospheric electrons by TC fields, as suggested by *Inan et al.* [1996], may lead to the production of detectable enhancements of 4.3-μm CO_2 emission. Model calculations for five different cases indicate that the strongest effects are expected for laterally extensive TC charge distributions, such as those associated with a MCS, and in cases where the atmospheric conductivity allows penetration of the electrostatic field to relatively high altitudes. Enhancements of CO_2 $T_{\rm vib}$ start near 70 km, with maximum enhancement of up to 50 K near 80 km altitude. As a result of IR-mediated radiative diffusion, the enhancements extend up into the thermosphere, well above 130 km, despite the fact that significant heating occurs only below 90 km. Limb-view broadband 4.3-μm enhancements of up to a factor of two above ambient nighttime levels are predicted for TH between 77 km and 120 km, with larger enhancements in selected narrower spectral regions. Somewhat larger enhancements would be expected if electron excitation of other molecular vibrational states were allowed, including direct excitation of CO_2 ν_3 and perhaps excitation of O_2(v), which is coupled to CO_2 ν_3 and N_2(v).

The fact that significant IR enhancements are only predicted to occur for Cases A4 and A5 underscores the dependence of the upward penetration of TC field on the profile of σ. Simple considerations of the E-field variation in an inhomogeneous medium indicate that effective penetration to ionospheric altitudes is maximized when the fewest e-foldings of σ occur between TC and ionosphere. Our results indicate that significant IR enhancements should occur when the σ profile lies in the range between P2 and P3. In view of the scarcity of *in situ* data, it is difficult to assess the geophysical conditions under which the conductivity profile would be similar to that described by profiles P2 or P3. However, rocket measurements [*Hale*, 1994] do indicate profile P3 to be a 'typical' mid-latitude nighttime profile. Thus we can reasonably expect that conditions leading to effective coupling and IR enhancements should occur at least some of the time.

The importance of having a spatially extensive MCS with area $\sim 10^4$ km^2 for obtaining E fields sufficient to excite N_2(v) is borne out by the rocket measurements of *Kelley et al.* [1985], showing E fields of only tens of mV/m above relatively small storm cells with horizontal extents $\sim$ 10-20 km, in contrast to the 1-10 V/m resulting from our calculations for charge distributions similar to those observed by *Marshall et al.* [1996]. The difference in E fields between relatively small cells and a MCS is demonstrated by U-2 aircraft measurements near $z = 20$ km over a large active storm [*Blakeslee et al.*, 1989]. These measurements reported $E =$ 1-7 kV/m, in agreement with our calculations for Cases A4 and A5, but greater than the balloonborne measurements associated with the rocket campaign of *Kelley et al.* [1985] at 21 km by a factor of 10^3 - 10^4.

Acknowledgments. We gratefully acknowledge the sponsorship of the Air Force Office of Scientific Research's Directorate of Mathematics and Geosciences and the encouragement of L. S. Jeong and W. A. M. Blumberg. Three of us (U.S.I., V.P.P., and P.P.W.) were supported under contracts with the Phillips Laboratory, Geophysics Directorate.

References

Blakeslee, R. J., H. J. Christian, and B. Vonnegut, *J. Geophys. Res., 94*, 13135-13140, 1989.
Brook, M., M. Nakano, P. Krehbiehl, and T. Takeuti, *J. Geophys. Res., 87*, 1207, 1982.
Hale, L. C., C. L. Croskey, and J. D. Mitchell, *Geophys. Res. Lett., 8*, 927, 1981.
Hale, L. C., *J. Geophys. Res., 99*, 21089, 1994.
Hampton, D. L., M. J. Heavner, E. M. Wescott, and D. D. Sentman, *Geophys. Res. Lett., 22*, 89, 1996.
Hays, P. B. and R. G. Roble, *J. Geophys. Res., 84*, 3291, 1979.
Inan, U. S., V. P. Pasko, and T. F. Bell, *Geophys. Res. Lett., 23*, 1067-1070, 1996.
Kelley, M. C., C. L. Siefring, R. F. Pfaff, P. M. Kintner, M. Larsen, R. Green, R. H. Holzworth, L. C. Hale, J. D. Mitchell, and D. Le Vine, *J. Geophys. Res., 90*, 9815-9823, 1985.
Kumer, J. B., *J. Geophys. Res., 82*, 2203, 1977.
Marshall, T. C., M. Stolzenburg, and W. D. Rust, *J. Geophys. Res., 101*, 6979- 6996, 1996.
Mende, S. B., R. L. Rairden, G. R. Swenson, and W. A. Lyons, *Geophys. Res. Lett., 22*, 2633, 1995.
Nebel, H., P. P. Wintersteiner, R. H. Picard, J. R. Winick, and R. D. Sharma, *J. Geophys. Res., 99*, 10409-10419, 1994.
Park, C. G., and M. Dejnakarintra, *J. Geophys. Res., 78*, 6623, 1973.
Pasko, V. P., U. S. Inan, and T. F. Bell, *J. Atm Terr. Phys.*, in review, 1996.
Pasko, V. P., U. S. Inan, T. F. Bell, and Y. N. Taranenko, *J. Geophys. Res., 102*, 4529, 1997.
Phelps, A. V., *Gaseous Dielectric, 5*, 1-9, 1987.
Roble, R. G., *J. Atm. Terr. Phys., 53*, 831, 1991.
Rothman, L. S., *et al.*, *J. Quant. Spectrosc. Radiat. Transfer, 48*, 469-507, 1992.
Taranenko, Y. N., U. S. Inan, and T. F. Bell, *Geophys. Res. Lett., 20*, 1539-1542, 1993.
Tzur, I., and R. G. Roble, *J. Geophys. Res., 90*, 5989, 1985.
Velinov, P. I., and P. T. Tonev, *J. Atm. Terr. Phys., 57*, 687, 1995.
Whalen, J. A., R. R. O'Neil, and R. H. Picard, The aurora, in *Handbook of Geophysics and the Space Environment*, edited by A. S. Jursa, Chapter 12, Air Force Geophys. Lab., Bedford, Mass., 1985.
Winick, J. R., R. H. Picard, R. D. Sharma, R. A. Joseph, and P. P. Wintersteiner, in R. Rodrigo, J. J. Lopez-Moreno, M. Lopez-Puertas, and A. Molina eds., *Progress in atmospheric physics*, pp 229-237, Kluwer Academic Publ., Dordrecht, Neth., 1988.
Wintersteiner, P. P., R. H. Picard, R. D. Sharma, J. R. Winick, and R. A. Joseph, *J. Geophys. Res., 97*, 18083-18117, 1992.

R. H. Picard and J. R. Winick, PL/GPOS, Hanscom AFB, MA 01731 (e-mail: picard@plh.af.mil, winick@pldac.plh.af.mil)
U. S. Inan and V. P. Pasko, STAR Laboratory, Stanford University, Stanford, CA 94305 (e-mail: inan@star.stanford.edu, pasko@nova.stanford.edu)
P. P. Wintersteiner, ARCON Corporation, 260 Bear Hill Road, Waltham, MA 02154 (e-mail: winters@arcon.com)

(Received May 14, 1997; revised July 30, 1997; accepted August 21, 1997.)